A New Robust Digital Control of an Induction Motor Supplied by a 3-Level Voltage Inverter for Electric Vehicle Applications

M. Bendjedia, K. A. Tehrani, Y. Azzouz
ELECTRONICS AND SYSTEMS GROUP, IRSEEM/ESIGELEC
Technopôle du Madrillet, Saint-Etienne du Rouvray, 76800, France.
Tel.: +33 / (2) – 32.91.58.58
Fax: +33 / (2) – 32.91.58.59
Moussa.Bendjedia@esigelec.fr, Kambiz.Tehrani@esigelec.fr, Yacine.Azzouz@esigelec.fr
URL: http://www.esigelec.fr

Acknowledgements

The authors would like to thank the region Haute-Normandie (Upper Normandy) and the « Fonds Européen de Développement Régional (FEDER) » for the financial support under VIRTUOSE project.

Keywords

«Induction motor», «Digital control», «Vector control», «Power converters for EV».

Abstract

This paper aims to provide a robust control system for an induction motor (IM) used in electric vehicle (EV). A digital RST controller is designed to reduce response time without overshoot speed. High-dynamic performance is obtained by using the indirect stator-flux-oriented control (ISFOC) and the space vector pulse width modulation (SVPWM). In this paper, a three level neutral-point-clamped (NPC) has been used for electric vehicle applications. Multilevel converters can generate the output voltages with very low distortion and can reduce the dv/dt stresses; moreover, electromagnetic compatibility (EMC) problems can be reduced. The simulation results show the robustness and effectiveness of the proposed approaches.

Introduction

To reduce greenhouse gas emissions generated by cars, many industrials are encouraged to develop electric (EV) or hybrid vehicles (HEV). One of the disadvantages of the EV is the energy storage because the batteries have a limited range, and take a long time to charge [1]. This work is part of the development of a new extended range of EV. When the batteries have been discharged, a gas engine powers an electric generator for several hundreds of miles. The batteries can also be charged by solar panels installed on the roof of the vehicle.

On the other hand, the EV drive systems require fast torque response and high efficiency over a wide speed range. The induction motors are widely used for electric propulsion because they are characterized by reliability ruggedness, low maintenance, low cost, and ability to operate in hostile environments [2]. A methodology for presizing the induction motor propulsion of an electric vehicle is proposed in [3].

The induction control system based on classical proportional integral derivative (PID) is no longer satisfies the operating conditions requirements of the EV. Therefore, advanced regulators must be used in order to fulfill these requirements. The RST controller is an efficient strategy of digital control and it has been used in many applications. For HEV, it has been applied to the DC/DC converter to ensure energy management between supercapacitor and battery [4]. In [5], the RST controller is designed to control the PWM rectifier for battery charger of the EV. The RST controller is also used in renewable energy systems [6] in order to regulate the wind turbine rotor speed. In [7], this controller has been

proposed to control the rotor position of the hybrid step motor where a high accuracy of positioning is required.

By using classical two-level inverter, significant amount of harmonic appear in the output voltage. This harmonics can cause severe torque pulsation, motor heating and electromagnetic interferences especially if a long power cable is used between the inverter and the motor [8]. Several methods based on passive filters have been proposed in the literature to reduce the harmonics and the overvoltage (dv/dt) at the motor terminals. In EV applications, these filters are not suitable because they increase size and weight of the system.

Multilevel-inverters are the promising alternative solutions for motor drive problems such as power quality and electromagnetic interferences especially in high-power application areas. The concept of utilizing multiple small voltage levels to perform power conversion was patented by an MIT researcher about thirty years ago [9]. Subsequently, many multilevel converter topologies have been developed [10]-[13]. The most commonly used multilevel inverter is the three-level NPC inverter [14]-[17]. Compared to the standard two-level inverter, the three-level inverter presents good power quality, highly reduced dv/dt stresses, low total harmonic distortions of load voltage also load current and the capability of an effective reduction of the homopolar voltage [14]-[17].
One of the most important requirements in the operation of multilevel NPC inverters is balancing capacitors voltages. The various methods have been proposed by the authors as [18].
In this paper, we propose a robust control system for an induction motor used in electric vehicle (EV). We designed an advanced RST controller for speed control. In order to obtain high-dynamic performance, we used the ISFOC and the SVPWM techniques. The induction motor is supplied by a three level NPC inverter.

Stator flux orientation control

According to the synchronous frame ($d-q$), the electrical induction motor dynamic model can be expressed by the following equations:

$$\frac{\mathrm{d}\Phi_{\mathrm{ds}}}{\mathrm{dt}} = \omega_s \Phi_{qs} - R_s i_{ds} + v_{ds} \tag{1}$$

$$\frac{\mathrm{d}\Phi_{\mathrm{qs}}}{\mathrm{dt}} = -\omega_s \Phi_{ds} - R_s i_{qs} + v_{qs} \tag{2}$$

$$\frac{\mathrm{di}_{\mathrm{ds}}}{\mathrm{dt}} = \frac{1}{\sigma \tau_{\mathrm{r}} L_s}\Phi_{ds} + \frac{\omega_r}{\sigma L_s}\Phi_{qs} - \frac{\left(\tau_{\mathrm{s}} + \tau_{\mathrm{r}}\right)}{\sigma \tau_{\mathrm{s}} \tau_{\mathrm{r}}} i_{ds} + \omega_{sl} i_{qs} + \frac{1}{\sigma L_s} v_{ds} \tag{3}$$

$$\frac{\mathrm{di}_{\mathrm{qs}}}{\mathrm{dt}} = -\frac{\omega_r}{\sigma L_s}\Phi_{ds} + \frac{1}{\sigma \tau_{\mathrm{r}} L_s}\Phi_{qs} - \omega_{sl} i_{ds} - \frac{\left(\tau_{\mathrm{s}} + \tau_{\mathrm{r}}\right)}{\sigma \tau_{\mathrm{s}} \tau_{\mathrm{r}}} i_{qs} + \frac{1}{\sigma L_s} v_{qs} \tag{4}$$

Where:

$\sigma = 1 - \frac{M^2}{L_{\mathrm{s}} L_{\mathrm{r}}}$, $\tau_s = \frac{L_{\mathrm{s}}}{R_{\mathrm{s}}}$: stator time constant, $\tau_r = \frac{L_{\mathrm{r}}}{R_{\mathrm{r}}}$: rotor time constant

v_{ds} and v_{qs} : d- and q- axis stator voltages [V].
i_{ds} and i_{qs} : d- and q- axis stator currents [A].
Φ_{ds} and Φ_{qs} : d- and q- axis stator *flux* [Wb].
R_s and R_r : Stator and rotor winding resistances [Ω].
L_s, L_r and M: Stator, rotor and mutual inductances [H].
ω_r and ω_{sl} : Rotor and slip angular speed [rad/s].

The electromagnetic torque can be expressed as follows:

$$T_e = N_p \left(\Phi_{ds} i_{qs} - \Phi_{qs} i_{ds} \right) \tag{5}$$

N_p is the number of the pole pairs.

For ISFOC, the d-axis is chosen on the flux axis, so all the flux is aligned along this axis, which means $\Phi_{ds} = \Phi_s$ and $\Phi_{qs} = 0$. It can be seen that if the stator flux is kept constant, the torque can be controlled by using the q-axis current, therefore, the equation (5) becomes

$$T_e = N_p \Phi_{ds} i_{qs} \tag{6}$$

The mechanical equation is given by

$$N_p \left(T_e - T_L \right) = J \frac{\mathrm{d}\omega_r}{\mathrm{dt}} + f \omega_r \tag{7}$$

Where:
J : Rotor inertia [kg.m²]
f : Viscous friction coefficient [N.m.s/rad]
T_L : Load torque [N.m]

Fig. 1 shows a simplified bloc diagram of the proposed control if induction motor.

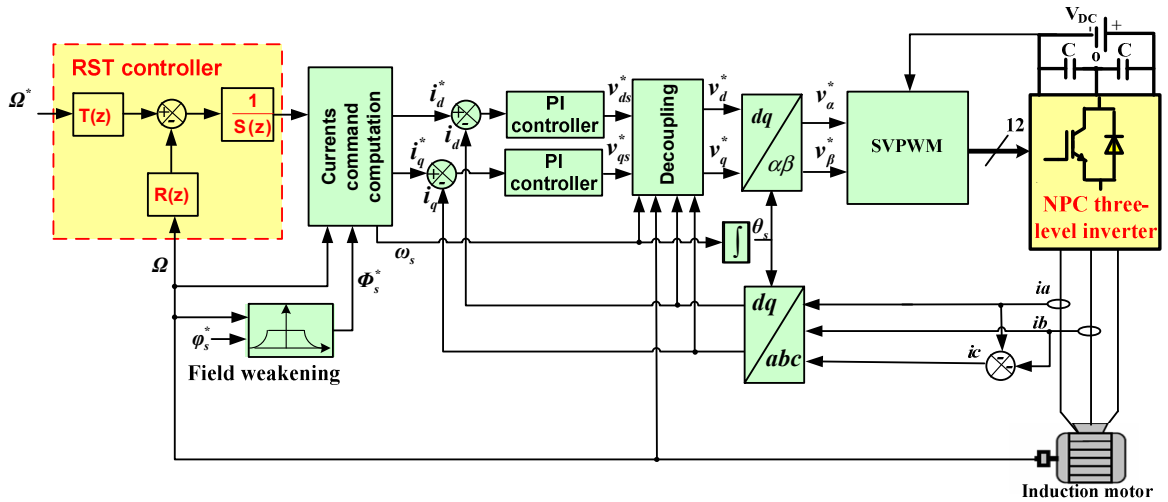

Fig. 1. Bloc diagram of the proposed drive system using RST controller and NPC three-level inverter

Where:
ω_s : synchronous angular speed [rad/s].
Ω : Mechanical rotor speed [rad/s].
θ_s: Electrical position [rad].
v_α and v_β: α- and β- axis stator voltages [V].
V_{DC} : Inverter input DC voltage [V].
C: Capacitor [F].

The d and q-axis command stator currents (8) are obtained by solving (1)-(4).

$$
\begin{aligned}
i_{ds}^{*} &= \frac{\left(1+\tau_r p\right)\Phi_s^{*} + L_s\sigma\tau_r\omega_{sl}i_{qs}^{*}}{L_s\left(1+\sigma\tau_r p\right)} \\
i_{qs}^{*} &= \frac{\tau_r\omega_{sl}\left(\Phi_s^{*} - L_s\sigma i_{ds}^{*}\right)}{L_s\left(1+\sigma\tau_r p\right)}
\end{aligned}
\tag{8}
$$

The flux command Φ_s^{*} is constant and the drive operates with constant torque. The drive can work in the field-weakening region by programming the flux as function of the speed as follow:

$$
\begin{aligned}
\Phi_s^{*} &= \phi_s^{*} \qquad if \quad |\Omega| < \Omega_n \\
\Phi_s^{*} &= \frac{\Omega_n\phi_s^{*}}{|\Omega|} \quad if \quad |\Omega| > \Omega_n
\end{aligned}
\tag{9}
$$

Ω_n is the nominal speed.

The *d* and *q*-axis command stator voltage can be expressed as:

$$
\begin{aligned}
v_{ds}^{*} &= \sigma L_s\left(p + \frac{\tau_s + \tau_r}{\sigma\tau_s\tau_r}\right)i_{ds}^{*} - e_d \\
v_{qs}^{*} &= \sigma L_s\left(p + \frac{\tau_s + \tau_r}{\sigma\tau_s\tau_r}\right)i_{qs}^{*} + e_q
\end{aligned}
\tag{10}
$$

Where $e_d = \frac{1}{\tau_r}\phi_s^{*} + \sigma L_s\omega_{sl}i_{qs}^{*}$ and $e_q = \frac{\omega_r}{\tau_r}\phi_s^{*} + \sigma L_s\omega_{sl}i_{ds}^{*}$ are the back electromotive force (EMF).

The *d* and *q*-axis command stator voltage should be produced as the outputs of the current controllers. However, these voltages are coupled by the *d*- and *q*- back EMF which can deteriorate the desired performance of the currents controllers. In order to have linear terms in (10), we applied the feedforward decoupling method [19].

RST controller design

The RST controller is proposed for speed control in order to improve the dynamic performance of the system drive. This polynomial controller is based on the bloc diagram shown in Fig. 2.

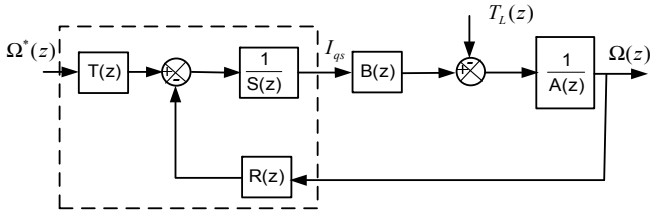

Fig. 2: Bloc diagram of the RST controller

In Fig. 2, $S(z)$, $R(z)$ and $T(z)$ are the polynomials of the RST controller. $B(z)$ and $A(z)$ are respectively the numerator and the denominator of the mechanical motor model. Thus, the closed loop system is given by:

$$\Omega = \frac{T(z)B(z)}{A(z)S(z)+B(z)R(z)}\Omega^* - \frac{A(z)S(z)}{A(z)S(z)+B(z)R(z)}T_L \tag{11}$$

The parameters of $S(z)$ and $R(z)$ can be obtained by solving the Diophantine equation defined by:

$$A(z)S(z)+B(z)R(z)=D(z) \tag{12}$$

$D(z)$ is the characteristic polynomial (i.e., the imposed poles in closed loop system).
Two conditions must be satisfied: a null steady state error and load torque disturbance rejection.

The first step in the design of RST controller is to obtain the discrete model of the system. By using (6) and (7), the mechanical model of IM, in the continuous domain, is given by

$$F(p)=\frac{\Omega(p)}{i_{qs}^*(p)}=\frac{K}{1+\tau p} \tag{13}$$

Where $K=\frac{N_p\Phi_s}{f}$ and $\tau=\frac{J}{f}$
The discrete time representation of the model in (13) can be obtained as follows

$$\frac{B(z)}{A(z)}=\frac{K\left(1-k_1\right)z^{-1}}{1-k_1z^{-1}} \tag{14}$$

with $k_1=e^{-\frac{T}{\tau}}$

The choice of the degrees of the polynomials is an important step in the design of the RST controller. It is a compromise between performance and complex controller. We choose a strictly proper controller in order to achieve a good accuracy adjustment. So the degrees of the polynomials are given by

$$\begin{aligned}&\deg(S(z))=\deg(A(z))+1=2\\&\deg(R(z))=\deg(A(z))=1\end{aligned} \tag{15}$$

By using (14) and (15), the $S(z)$ and $R(z)$ can be expressed as follow

$$\begin{aligned}&S(z)=(1-z^{-1})(s_0+s_1z^{-1})\\&R(z)=r_0+r_1z^{-1}\end{aligned} \tag{16}$$

In order to cancel the effect of load torque disturbance (11), an integration action is introduced in *S(z)*.

The choice of the imposed poles is done according to the desired performances for the closed loop system. In order to have fast speed time response without overshoot, we choose the following poles in the continuous domain.

$$\begin{aligned}&p_{1,2}=-\zeta\omega_0\pm j\zeta\omega_0\\&p_3=-\zeta\omega_0\end{aligned} \tag{17}$$

With ζ = *0.707*: Damping coefficient, ω_0 : Natural frequency

In the pair of complex conjugate poles (17), the imaginary part is equal to the negative real part and the third pole also is equal to the negative real part. In this case, the overshoot created by the pair of the complex conjugate poles is compensated by the real pole.
The transformation of the imposed poles (17) to the discrete plan leads to the polynomial $P(z)$ of (12) as follows

$$D(z) = d_0 + d_1 z^{-1} + d_2 z^{-2} + d_3 z^{-3} \tag{18}$$

Where:
$d_0 = 1$, $d_1 = -e^{-\zeta\omega_0 T}\left(2\cos(\omega_a T)+1\right)$, $d_2 = e^{-2\zeta\omega_0 T}\left(2\cos(\omega_a T)+1\right)$, $d_3 = -e^{-3\zeta\omega_0 T}$ and $\omega_a = \omega_0\sqrt{1-\zeta^2}$

Therefore, the coefficients of $S(z)$ and $R(z)$ can be found by resolution of the following system.

$$\begin{bmatrix} 1 & 0 & 0 & 0 \\ -(1+k_1) & 1 & K(1-k_1) & 0 \\ k_1 & -(1+k_1) & 0 & K(1-k_1) \\ 0 & k_1 & 0 & 0 \end{bmatrix} \begin{bmatrix} s_0 \\ s_1 \\ r_0 \\ r_1 \end{bmatrix} = \begin{bmatrix} d_0 \\ d_1 \\ d_2 \\ d_3 \end{bmatrix} \tag{19}$$

The polynomial $T(z)$ can be a constant that guarantee a unit gain of the closed loop system (11) which become

$$\Omega = \frac{T(1)}{R(1)}\Omega^* \tag{20}$$

That leads to the polynomial $T(z)$

$$\mathrm{T(z) = t_0 = r_0 + r_1} \tag{21}$$

NPC three - level inverter

The main circuit of 3-level NPC inverter is presented in Fig. 3. Each leg of the inverter is composed of four IGBT transistors with anti-parallel diodes and two clamping diodes connected to the midpoint O. In this case, three states of the output voltage are obtained: +VDC/2, O, and -VDC/2, resulting in additional voltage levels while reducing the voltage stress on the individual transistors. In order to avoid the unbalanced DC link capacitors voltages problem, we used two separated power sources VDC/2 as shown in Fig. 3

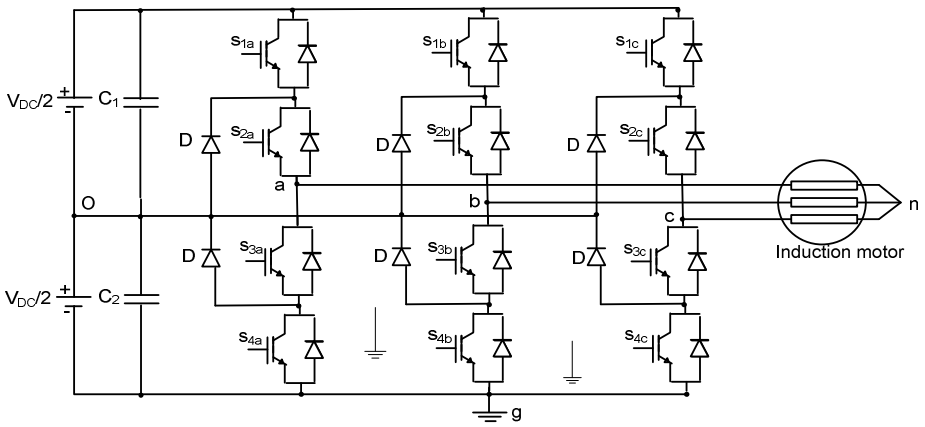

Fig. 3: NPC three-level inverter fed induction motor

In a 3-level NPC inverter, switching states s_a , s_b , and s_c are defined for the *a*- *b*- and *c*-phase respectively. Each switching state has a range from 0 to (*k*-1), in order to represent the complete number of switching levels.

The output line-to-ground voltages are obtained by:

$$\begin{bmatrix} v_{ag} \\ v_{bg} \\ v_{cg} \end{bmatrix} = \left(\frac{V_{DC}}{k-1} \right) \begin{bmatrix} s_a \\ s_b \\ s_c \end{bmatrix} \tag{22}$$

Where k is the number of levels.

We can also find the inverter line-to-line voltages; these are related to the line-to-ground voltages by:

$$\begin{bmatrix} v_{ab} \\ v_{bc} \\ v_{ca} \end{bmatrix} = \begin{bmatrix} 1 & -1 & 0 \\ 0 & 1 & -1 \\ -1 & 0 & 1 \end{bmatrix} \begin{bmatrix} v_{ag} \\ v_{bg} \\ v_{cg} \end{bmatrix} \tag{23}$$

The line-to-neutral voltages may be determined directly from the line-to-ground voltages as follows:

$$\begin{bmatrix} v_{an} \\ v_{bn} \\ v_{cn} \end{bmatrix} = \begin{bmatrix} 2 & -1 & -1 \\ -1 & 2 & -1 \\ -1 & -1 & 2 \end{bmatrix} \begin{bmatrix} v_{ag} \\ v_{bg} \\ v_{cg} \end{bmatrix} \tag{24}$$

The inverter voltages can be expressed in the arbitrary *q*-*d* reference frame by:

$$\begin{bmatrix} v_{qn} \\ v_{dn} \\ v_{on} \end{bmatrix} = \begin{bmatrix} \cos(\theta) & \cos\left(\theta - \frac{2\pi}{3}\right) & \cos\left(\theta + \frac{2\pi}{3}\right) \\ \sin(\theta) & \sin\left(\theta - \frac{2\pi}{3}\right) & \sin\left(\theta + \frac{2\pi}{3}\right) \\ \frac{1}{2} & \frac{1}{2} & \frac{1}{2} \end{bmatrix} \begin{bmatrix} v_{an} \\ v_{bn} \\ v_{cn} \end{bmatrix} \tag{25}$$

To improve the dynamic performance of the overall control system, we used the SVPWM technique instead of classical carrier-based PWM. Comparison between these two techniques can be found in [20], [21]. The SVPWM is based on space vector representation of the voltages in the α-β plane by using Clark's transformation. The SVPWM is characterized by lower switching loss, lower ripple, lower total harmonic distortion in the motor current and better DC bus utilization.

Simulation results

This section presents the simulation results obtained from speed control of IM drives supplied by a 3-level voltage inverter as shown in Fig. 1. The simulation is realized with the Matlab/Simulink software environment including the SimPowerSystems libraries. The RST controller is designed in the discrete time (z-domain). Therefore, the system shown in Fig. 1 is transformed in this domain. The IM parameters are given in table I. The total sampling time is 62.5 µs. The choice of the parameters of currents controllers is done according to the desired performances for the closed loop system by imposing the natural frequency and the damping ratio.

Fig. 4 and Fig. 5 show an example of simulation results of speed control of induction supplied by 3-level Inverter. The speed reference is 1430 rpm and the load torque T_L = 15 Nm is applied at t = 1 s and removed at t = 2 s.

For comparison with the RST controller, we presented in Fig. 4, the speed time response obtained by using an integral-proportional (IP) controller [18]. It can be seen that IP and RST controllers are more suitable to overcome the problems of overshoot and instability. However, the RST controller is better, in terms of rapidity and load torque disturbance rejection.
Fig. 5 (a) shows that the motor torque is controlled by the *q*-axis current (ISFOC) as given in (6). In Fig. 5 (b) and (c) we presented the stator currents in the *d-q* axis reference frame and the fixed reference frame (*a,b,c*) respectively. By using the SVPWM and the 3-level inverter, the motor currents are less noisy. As shown in Fig. 5 (d) and (e), the motor voltages contain different levels allowing low total harmonic distortion (THD) as illustrated in Fig. 5 (f). On the other hand the blocking voltage of each IGBT transistor is clamped to the half of DC-link voltage.

Table I: Induction motor parameters

Specifications		Parameters	
Rated power	3kW	Stator resistance: R_s	2.3 Ω
Rated voltage	380V	Rotor resistance: R_r	1.55 Ω
Rated current	6.6A	Stator inductance: L_s	0.261 H
Rated frequency	50Hz	Rotor inductance: L_r	0.261 H
Number of pole pairs	2	Mutual inductance: M	0.249 H
Rated speed	1430 r/min	Motor inertia: J	0.02 kg/m^2
		Viscous friction coefficient: f	0.0007 Nm.s./rad

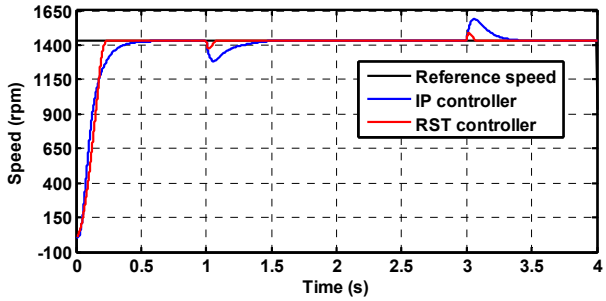

Fig. 4: Speed time response with IP and RST controller

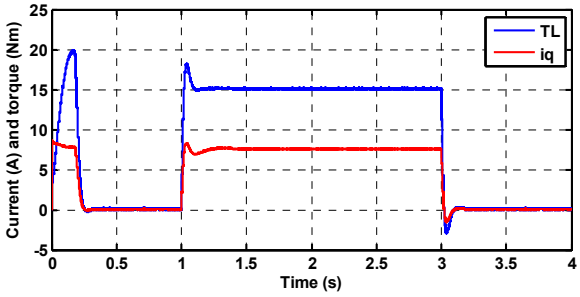

(a) *q* –axis stator current (i_q) and load torque (T_L)

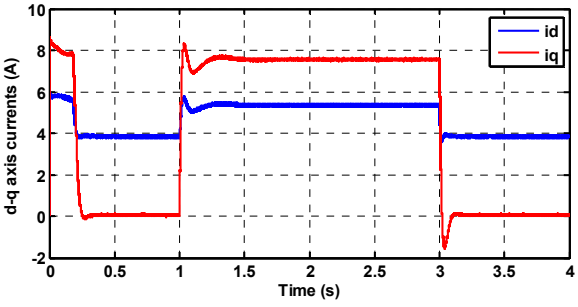

(b) *d-q* –axis stator currents (i_d, i_q)

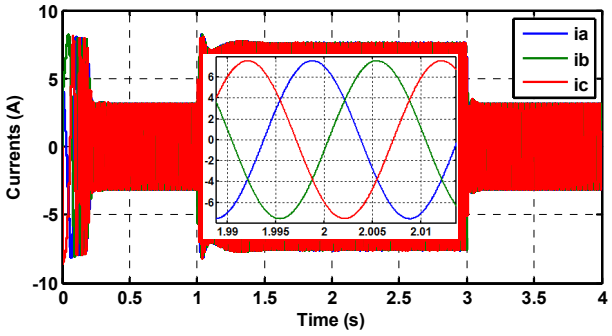

(c) Stator phase current (i_a, i_b, i_c)

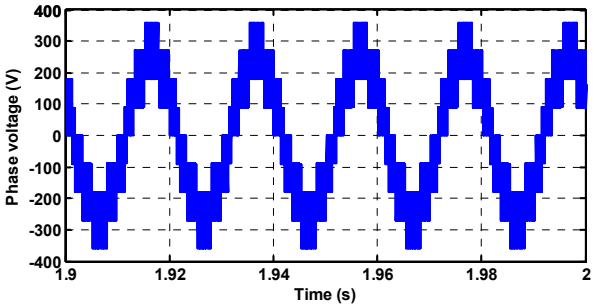

(d) Line-to-motor neutral point stator voltage (V_{an})

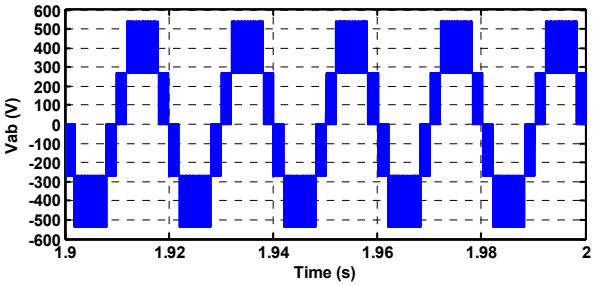

(e) Line-to-line stator voltage (V_{ab}) with 3-level Inverter

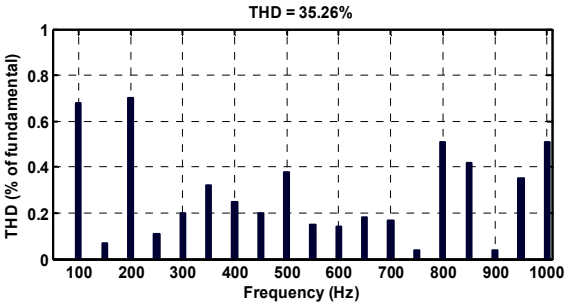

(f) THD of line-to-line stator voltage (V_{ab}) with 3-level Inverter

Fig. 5: Simulation results with RST controller of induction motor supplied by a 3-level voltage Inverter

Conclusion

In this paper a robust control system for induction motor drive fed by a three level NPC inverter is proposed for EV application. High-dynamic performance is obtained using the indirect stator-flux-oriented control (ISFOC) and the space vector pulse width modulation (SVPWM) techniques. An advanced RST controller is designed for speed control loop. This controller can accelerate the response time without overshoot thanks to proper poles placement of the closed loop system.

The 3-level inverter presents good power quality, highly reduced dv/dt stresses, low total harmonic distortions. Moreover, the unbalance DC voltage problem is solved by separate DC sources. In electric vehicle applications, the 3-level inverter can reduce the EMI noise that can easily diffuse into other electric devices due to the high-density packaging structure.

Simulation results show the advantage of the RST controller in comparison to classical controller, in terms of tracking and load torque disturbance rejection. By using the 3-level inverter, the THD of the motor voltage and current is reduced

References

[1] Jensen H. B., Schaltz E., Koustrup P. S., Andreasen S. J., Kaer S. K.: Evaluation of fuel-cell range extender impact on hybrid electrical vehicle performance, IEEE Trans. Veh. Techno. Vol. 62 no 1, Jan. 2013, pp. 50-60

[2] Zeraoulia M., Benbouzid M. E. H., Diallo D.: Electric motor drive selection issues for HEV propulsion systems: A comparative study, IEEE Trans. Veh. Techno., Vol. 55, no 6, Nov. 2006, pp. 1756-1764

[3] Tabbache B, Kheloui A., Benbouzid M. E. H., Diallo D.: Design and control of the induction motor propulsion of an electric vehicle, in Proc. IEEE/VPPC Conf., Sep. 2010, pp. 1–6

[4] Camara M. B., Gualous H., Gustin F., Berthon A., Dakyo B.: DC/DC converter design for supercapacitor and battery power management in hybrid vehicle applications - polynomial control strategy, IEEE Trans. Ind. Electron. Vol. 57, no 2, Feb. 2010, pp. 587-597

[5] Lacroix S., Hilairet M., Laboure E.: Design of a battery-charger controller for electric vehicle based on RST controller, in Proc. VPPC' 11 Conf., Sep. 2011, pp. 1–6

[6] Pintea A., Popescu D., Borne P.: Robust control for wind power systems, in Proc. MED'10 Conf., 23-25 June 2010, pp. 1085-1091

[7] Bendjedia M., Aït-Amirat Y., Walther B., Berthon A.: Digital step motor drive with EKF estimation of speed and rotor position, IREE Journal Vol. 2, no 3, May-June 2007, pp. 455-465

[8] Bendjedia M., Khlaief A., Boussak B.: Sensorless speed control of an outrunner PMSM drive connected to long cable for flying remote operative vehicle, in Proc. ICEM' 12 Conf., 2-5 Sep. 2012, pp. 2252-2258

[9] Baker R.H.: Electric power converter, U.S. Patent Number 3.867.643, Feb. 1975, Feb 1975

[10] Celanovic N.: Space vector modulation and control of multilevel converters, PhD Thesis, Virginia Polytechnic Institute, Mar. 2000

[11] Rodriguez J., Bernet S., Bin W., Pontt J., and Kouro S.: Multilevel voltage source-converter topologies for industrial medium-voltage drives, IEEE Trans. Ind. Electron. Vol. 54, no 6, Dec. 2007, pp. 2930-2945

[12] Tehrani K. A., Rasoanarivo I., Andriatsioharana H., Sargos. F.M.: A new multilevel inverter model NP without clamping diodes, in Proc IECON' 08 Conf., 10-13 Nov. 2008, pp. 466-472

[13] Kouro S. et al.: Recent advances and industrial applications of multilevel converters," IEEE Trans. Ind. Electron. Vol. 57, no. 8, , Aug. 2010, pp. 2553-2580

[14] Dordevic O., Levi E., Jones M.: A vector space decomposition based space vector PWM algorithm for a three-level seven-phase voltage source inverter, IEEE Trans. Power. Electron. Vol. 28, no 2, Feb. 2013, pp. 637-649

[15] Maheshwari R., Munk-Nielsen S., Busquets-Monge S.: Design of neutral-point voltage controller of a three-level NPC Inverter with small DC-link capacitors, IEEE Trans. Ind. Electron. Vol. 60, no 5, June. 2012, pp. 1861-1871

[16] Zhao Z., Zhong Y., Gao H., Yuan L., Lu T.: Hybrid selective harmonic elimination PWM for common-mode voltage reduction in three-level neutral-point-clamped inverters for variable speed induction drive, IEEE Trans. Power. Electron. Vol. 27, no 3, Mar. 2012, pp. 1152-1158

[17] Zhang Y., Zhu J., Zhao Z., Xu W., Dorrell D. G., "An improved direct torque control for three-level inverter-fed induction motor sensorless drive," IEEE Trans. Power. Electron. Vol. 27, no. 3, Mar. 2012, pp. 1502-1513

[18] Busquets-Monge S., Alepuz S., Bordonau J., Peracaula J.: Voltage balancing control of diode-clamped multilevel converters with passive front-ends, IEEE Trans. Power Electron. Vol. 23, no. 4, Jul. 2008, pp. 1751-1758.

[19] Boussak M., Jarray K.:A high-performance sensorless indirect stator flux orientation control of induction motor drive, IEEE Trans. Ind. Electron. Vol. 53, no. 1, Feb. 2006, pp. 41-49

[20] Yao W., Hu H., Lu Z.: Comparisons of space-vector modulation and carrier-based modulation of multilevel inverter, IEEE Trans. Power Electron. Vol. 23, no. 1, Jan. 2008, pp. 45–51

[21] Iqbal A., Moinuddin S.: Comprehensive relationship between carrier-based PWM and space vector PWM in a five-phase VSI, IEEE Trans. Power. Electron. Vol. 24, no 10, Oct. 2009, pp. 2379-2390